AGU PUBLICATIONS

JGR

Journal of Geophysical Research: Earth Surface

RESEARCH ARTICLE
10.1002/2015JF003658

Key Points:
- New type of seismic source is identified in the East Antarctic Ice Sheet
- The events are located within the upper 20 m of the firn layer
- Firnquakes are most likely associated with small-scale crevassing found on wind-glazed surfaces

Correspondence to:
A. C. Lough,
alough@dtm.ciw.edu

Citation:
Lough, A. C., C. G. Barcheck, D. A. Wiens, A. Nyblade, and S. Anandakrishnan (2015), A previously unreported type of seismic source in the firn layer of the East Antarctic Ice Sheet, *J. Geophys. Res. Earth Surf.*, *120*, 2237–2252, doi:10.1002/2015JF003658.

Received 26 JUN 2015
Accepted 11 OCT 2015
Accepted article online 14 OCT 2015
Published online 11 NOV 2015

©2015. American Geophysical Union. All Rights Reserved.

A previously unreported type of seismic source in the firn layer of the East Antarctic Ice Sheet

Amanda C. Lough[1,2], C. Grace Barcheck[2,3], Douglas A. Wiens[2], Andrew Nyblade[4], and Sridhar Anandakrishnan[4]

[1]Now at Department of Terrestrial Magnetism, Carnegie Institution for Science, Washington, District of Columbia, USA, [2]Department of Earth and Planetary Sciences, Washington University, St. Louis, Missouri, USA, [3]Now at Department of Earth and Planetary Sciences, University of California-Santa Cruz, Santa Cruz, California, USA, [4]Department of Geosciences, Pennsylvania State University, University Park, Pennsylvania, USA

Abstract We identify a unique type of seismic source in the uppermost part of the East Antarctic Ice Sheet recorded by temporary broadband seismic arrays in East Antarctica. These sources, termed "firnquakes," are characterized by dispersed surface wave trains with frequencies of 1–10 Hz detectable at distances up to 1000 km. Events show strong dispersed Rayleigh wave trains and an absence of observable body wave arrivals; most events also show weaker Love waves. Initial events were discovered by standard detection schemes; additional events were then detected with a correlation scanner using the initial arrivals as templates. We locate sources by determining the L2 misfit for a grid of potential source locations using Rayleigh wave arrival times and polarization directions. We then perform a multiple-filter analysis to calculate the Rayleigh wave group velocity dispersion and invert the group velocity for shear velocity structure. The resulting velocity structure is used as an input model to calculate synthetic seismograms. Inverting the dispersion curves yields ice velocity structures consistent with a low-velocity firn layer ~100 m thick and show that velocity structure is laterally variable. The absence of observable body wave phases and the relative amplitudes of Rayleigh waves and noise constrain the source depth to be less than 20 m. The presence of Love waves for most events suggests the source is not isotropic. We propose the events are linked to the formation of small crevasses in the firn, and several events correlate with shallow crevasse fields mapped in satellite imagery.

1. Introduction

A wide variety of different types of seismicity associated with glaciers and ice sheets (so-called icequakes) have been documented in the scientific literature. Icequakes occur when glacial ice experiences brittle deformation resulting in the outward radiation of seismic energy in the form of elastic waves, similar to traditional earthquakes. Glaciers (including those in the Transantarctic Mountains (TAM) and other alpine regions) experience high rates of low-magnitude ($M < 2$) seismicity that is often recordable within the noise environment only at local distances (1–10 km).

Probably the most common type of icequake, observed in a variety of settings, is that caused by surface cracking and crevassing [*Neave and Savage*, 1970]. Seismicity is also often associated with crevasse formation and propagation [*Walter et al.,* 2009; *Mikesell et al.,* 2012; *Röösli et al.,* 2014]. Icequakes associated with basal slip or tensile fracture are quite common and often correlate with changes in subglacial water pressure [*Anandakrishnan and Bentley*, 1993; *Walter et al.,* 2008]. In Norway, seismicity has been associated with accelerated basal slipping directly linked to an increase in intake from surface melt [*Moore et al.,* 2013]. In Switzerland, seismicity has been recorded associated with both surface runoff [*Canassy et al.,* 2012] and following the outburst of a glacier dammed lake [*Roux et al.,* 2010]. In Greenland, seismicity has been associated with supraglacial lake drainage events [*Carmichael et al.,* 2015]. At Taylor Glacier in Antarctica, seismic multiplets triggered by melt are used as a proxy for melt production [*Carmichael et al.,* 2012]. Icequakes commonly occur as multiplets or repeating events in a variety of settings including outlet glaciers [*Zoet et al.,* 2012]. A single region can demonstrate different types of repeating icequakes, such as Mount Rainier where they can be shallow and low frequency representing stick-slip motion at the base of alpine glaciers [*Thelen et al.,* 2013] or they can be low-frequency events located high on the edifice and triggered by snow loading [*Allstadt and Malone*, 2014]. The bases of alpine glaciers are also susceptible to tensile stresses that produce near-horizontal faults in basal ice layers [*Walter et al.,* 2010].

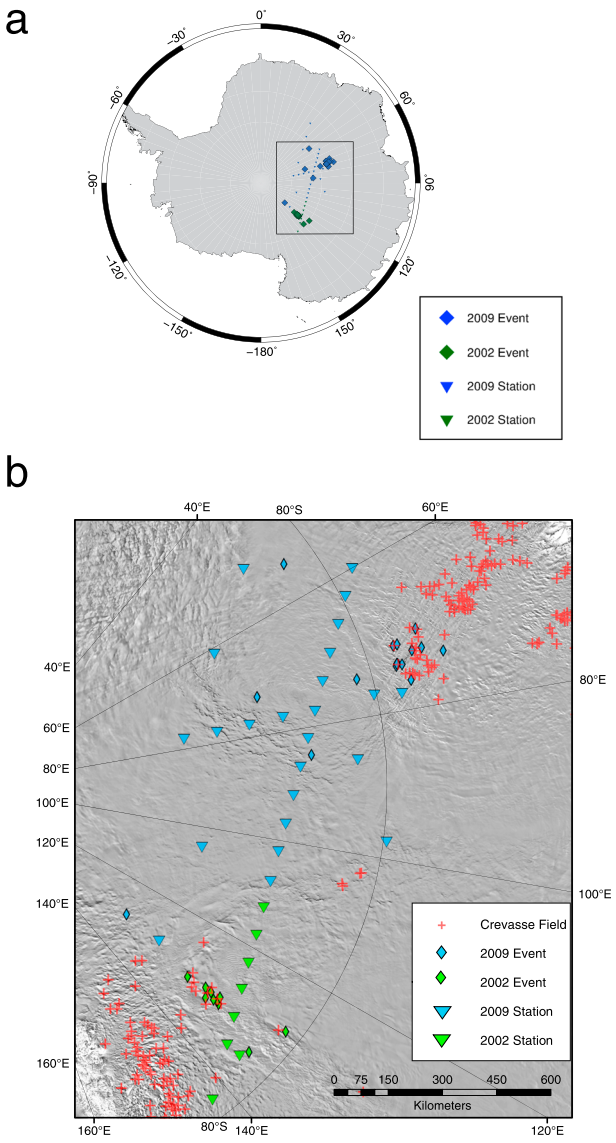

Figure 1. Location of seismic stations and events. (a) Map showing location of events and location of stations used in study. Box shows extent of Figure 1b. (b) Detailed map of events and stations plotted over Mosaic of Antarctica (MOA) [*Scambos et al.,* 2007]. Red crosses show locations of mapped crevasses by Byers, et al. (manuscript in preparation, 2015).

Alpine glaciers can experience precursory seismicity to large ice movements such as ice avalanches as seen on Iliamna volcano in Alaska [*Caplan-Auerbach and Huggel*, 2007]. Seismicity has been observed in areas beyond alpine glaciers such as events associated with propagating rifts in ice shelves [*Heeszel et al.,* 2014]. Outlet glaciers are another typical icequake location and can produce repeating rupture from asperities [*Bannister and Kennett*, 2002; *Danesi et al.,* 2007; *Zoet et al.,* 2012] or in other cases microseismicity [*West et al.,* 2010; *Byers et al.,* 2013]. Seismic energy from icequakes can be used to constrain the seismic velocity of glaciers and ice sheets [e.g., *Walter et al.*, 2015].

Outlet glaciers can also experience a completely different type of ice seismicity that is observed teleseismically in the long period (30–150 s) band [*Ekström et al.,* 2003; *Tsai et al.,* 2008; *Chen et al.,* 2011; *Bartholomaus et al.,* 2012; *Walter et al.,* 2012]. *Tsai and Ekström* [2007] identified numerous slow glacial earthquakes on Greenland tidewater outlet glaciers and *Nettles and Ekström* [2010] identified several Antarctic slow events that appear to result from calving processes. In Antarctica a new type of large-scale long period ice seismicity has been identified on the Whillans Ice Stream associated with the tidally modulated stick-slip motion at the base of the ice stream [*Wiens et al.,* 2008; *Walter et al.,* 2011; *Winberry et al.,* 2011, 2013; *Pratt et al.,* 2014].

Most ice seismicity can only be well studied in areas where local or regional seismic networks have been deployed. Unfortunately, large ice sheets such as the interiors of Antarctica and Greenland present logistical and environmental challenges to seismic deployments and so have not been well instrumented. However, recent technological developments permit the operation of autonomous seismographs on remote ice sheets for extended periods of time, allowing previously unstudied parts of the Antarctic interior to be instrumented and monitored. This study makes use of 26 seismographs operated from late 2008 to late 2009 on the East Antarctic interior, including in most cases over the winter, as part of the Gamburtsev Subglacial Mountains Seismic Experiment (GAMSEIS) component of the broader Antarctica's Gamburtsev Province (AGAP) initiative [*Hansen et al.,* 2010; *Heeszel et al.,* 2013] (Figure 1). The improvement in instrumentation, increase in the number of sensors, and decreased distance to potential source locations allow detection and study of seismic sources associated with the cryosphere over large regions and at lower magnitude levels than was previously possible.

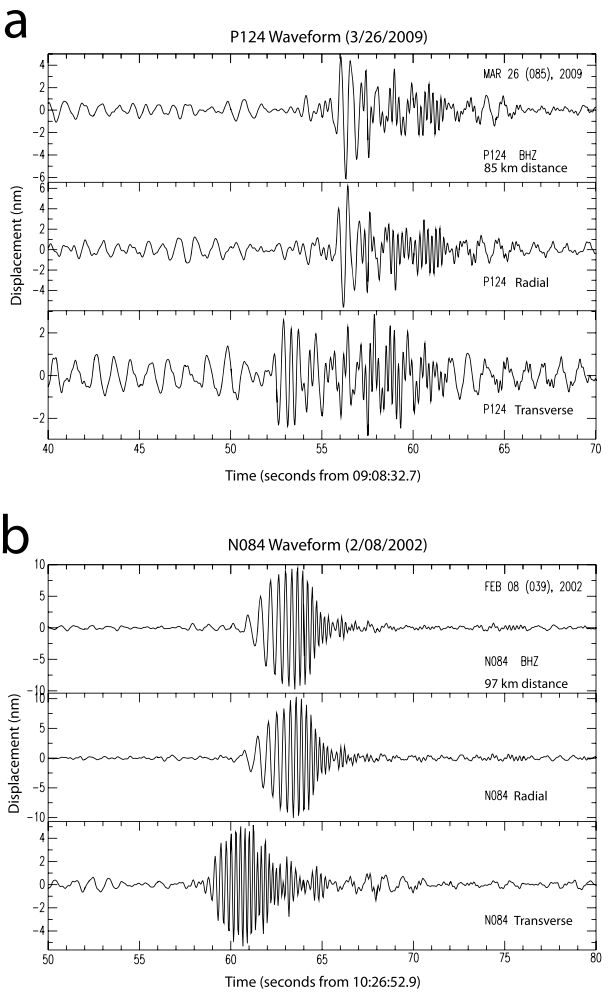

Figure 2. Examples of waveforms from several station/event pairings. Dispersed Rayleigh waves are clearly visible on both vertical and radial components while weaker Love waves are visible as earlier arrivals on the transverse components. Signals are band-pass filtered between 1 and 5 Hz. Time scales on the *x* axis are relative to the event origin time.

Here we identify a previously unreported type of icequake, characterized by high-frequency (1–10 Hz) seismic surface waves traveling in the East Antarctic Ice Sheet (Figure 2). These events have distinctive seismic waveforms, including the complete absence of visually observable body waves. Some events show only Rayleigh waves, whereas others show both Rayleigh and Love waves. The group velocities of the Rayleigh wave arrivals are on the order of 1.7 km/s, consistent with the expected propagation velocity of Rayleigh waves in ice. Dispersion is apparent on all waveforms (Figure 2) but the frequency range varies from event to event, with most showing amplitudes above the noise level at frequencies from 1 to 5 Hz, and higher frequencies observable for some events. Several events are large enough to be detected across the entire GAMSEIS array (nearly 1000 km, Figures 3 and 4), whereas others are only observed on the closest stations (several hundred kilometers). Similar, albeit smaller events located in East Antarctica about 400 km west of the Miller Range of the TAM were recorded by instruments deployed as part of the Transantarctic Seismic Experiment (TAMSEIS, 2001–2003) experiment (Figure 5). Additional events in this region with similar waveforms were triggered by surface waves from the 2010 M_w 8.8 Maule earthquake in Chile [*Peng et al.,* 2014].

Surface waves with sufficient energy to be detectable across several hundred kilometers of ice sheet have not been previously identified in the literature, and so their source represents a new type of ice seismicity. Here we describe the characteristics of these ice events and in particular analyze in detail the two best recorded events during the GAMSEIS deployment. We will show that these events represent faulting or cracking within the shallowest part of the firn layer and suggest that they accompany the formation of small crevasse fields observed in the shallow firn layer, particularly in wind-glazed regions surrounding the central part of East Antarctica. We use the term "firnquake" for these newly observed seismic sources because they are highly energetic sources that clearly occur in the firn layer. The term "firn quake" or firnquake has previously been used to describe several types of sudden phenomena within the firn layer, including "whumpfs" [*Sorge*, 1933; *Den Hartog*, 1982; *Johnson et al.,* 2005; *Heierli*, 2005], which are sudden collapses within the firn layer. In this paper we use this term without any assumption about the source mechanism but will review possible interpretations in the discussion section.

2. Data

This study primarily uses data from the AGAP/GAMSEIS project recorded between December 2008 and December 2009, with additional analysis of some events recorded by the TAMSEIS project in 2002. The US component of the GAMSEIS project installed 24 seismic stations in the Gamburtsev Mountains of

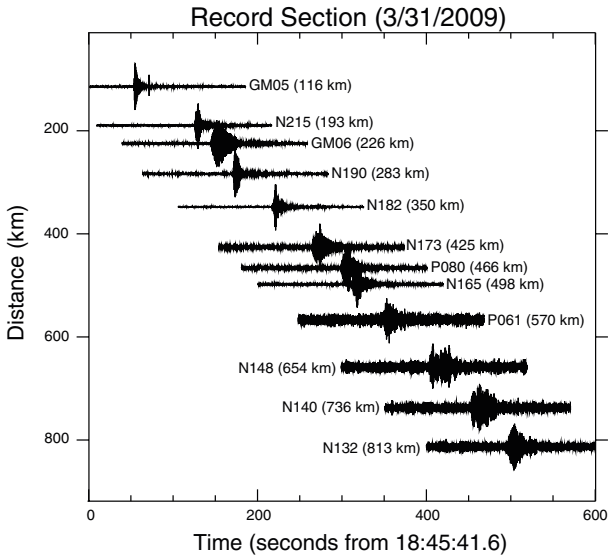

Figure 3. Record section for event on 31 March 2009. Vertical component waveforms have been band-pass filtered between 1 and 5 Hz. Time scale on the *x* axis is relative to the event origin time. *Y* axis is proportional to distance to event epicenter (km).

East Antarctica (Figures 1 and 4) with the intent to determine the uplift and support mechanisms of the subglacial mountain range [*Hansen et al.,* 2010; *Heeszel et al.,* 2013]. Each station included a broadband seismic sensor installed on a leveled pad with a fiberglass insulating cover beneath a rigid protective dome, at a depth of about 1 m below the snow surface. GAMSEIS stations utilized one of two types of sensors: either Guralp cold-weather 3T or Trillium T-240 instruments. Data were recorded by a Quanterra Q-330 data logger at 40 Hz and 1 Hz sample rates. The equipment was powered by lead acid batteries recharged by solar panels over the austral summer and primary lithium batteries over the winter, with the batteries and data logger housed in an insulating box. A Xeos iridium modem provided state of health information and small samples of 1 Hz data via satellite connection. Most of the stations operated successfully over the Antarctic winter, and data return for 2008–2009 was about 90% of the possible data.

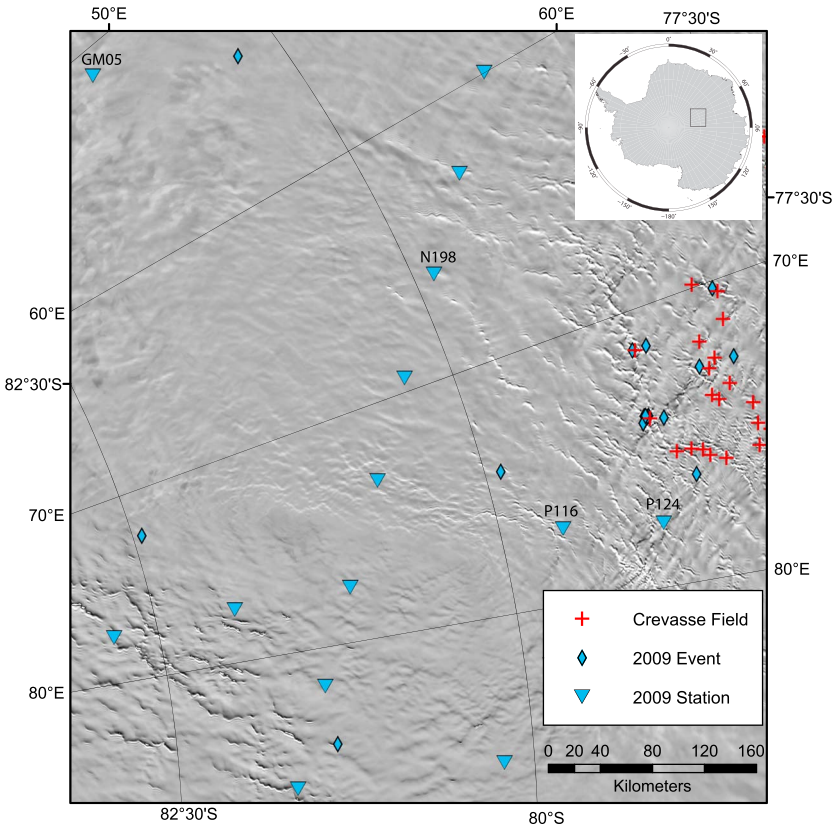

Figure 4. Detailed map of 2009 events and stations plotted over MOA [*Scambos et al.,* 2007]. Red crosses show locations of mapped crevasses by *Byers et al.* [2013].

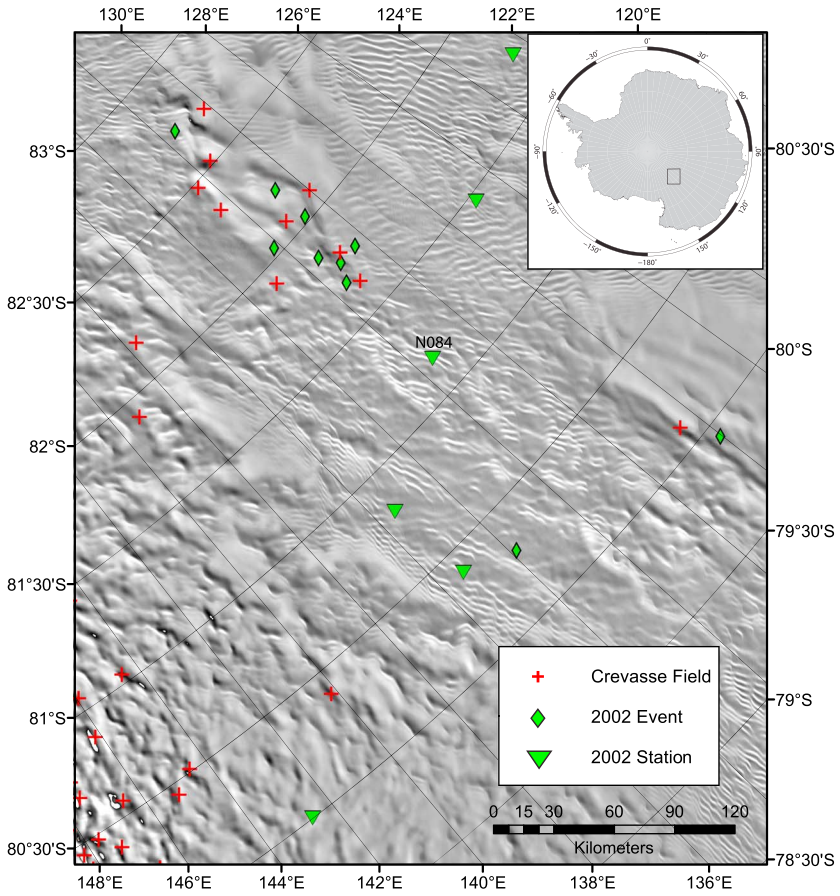

Figure 5. Detailed map of 2002 events and stations plotted over MOA [*Scambos et al.,* 2007]. Red crosses show locations of mapped crevasses by *Byers et al.* [2013].

We also locate and discuss firnquakes recorded by the TAMSEIS project in 2002, which had been noted earlier during that experiment but were not recorded well enough for a complete study at that time. TAMSEIS seismic stations were an earlier generation of the polar seismic instrumentation and used standard Guralp 3T sensors and Reftek RT72-08 data loggers [*Barklage et al.,* 2009]. Lithium batteries were not available so lead acid batteries were used and recharged by solar panels and wind turbines. These limitations in power meant TAMSEIS stations could only run when solar power was available to recharge the batteries, thereby limiting continuous data collection only to 4 or 5 months of austral summer each year. TAMSEIS data in this study covers January to March 2002 and is limited to six stations (approximately 400 km; Figure 1). TAMSEIS stations are situated in a linear pattern (Figures 1 and 5), which leads to poor location accuracy; therefore, we have limited our analysis of the TAMSEIS events to approximate source epicenter and magnitude.

3. Methods

3.1. Detection and Location

We analyzed the 2009 GAMSEIS data for seismicity using the short-term average long-term average event detector in the Antelope software package [*Harvey*, 2003]. We first discovered the firnquakes when locations could not be determined assuming the detected arrivals were conventional *P* or *S* wave arrivals. Closer inspection revealed that the arrivals consisted of Rayleigh waves, as indicated by the retrograde, elliptical particle motions confined to the source-to-receiver plane.

We then located the events using a grid search algorithm that minimized the L2 misfit in predicted arrival times, assuming velocities appropriate for Rayleigh waves propagating in the ice sheet. The first Rayleigh wave arrival time on the vertical component was picked (reminiscent of *P* wave picking in traditional location

algorithms) with a quality of A, B, or C assigned based on the reliability of the pick which was then factored into the error weighting. We initially assumed that the Rayleigh waves traveled at the 1 Hz group velocity appropriate for the shear wave velocity structure of the South Pole [*Albert*, 1998]. For well-recorded events, we also performed a grid search over the Rayleigh wave group velocity to determine if a different velocity might lead to a better fit. Overall, we found 1.7 ± 0.5 km/s to be an appropriate average group velocity, although other similar velocities produce only very small changes in event location and origin time. We first used an equidistant grid of 0.3° (approximately 33 km) centered near the geographic South Pole covering the entire Antarctic continent to determine an initial location. We then refined the search using a denser grid spacing of 0.05° (approximately 5 km) or 0.02° (approximately 2 km) centered at the initial location for well-recorded events.

The events recorded in 2002 by TAMSEIS were initially identified as unusual arrivals but they could not be well located and characterized due to the linear array geometry. In this study we reanalyze all the previously identified events, some of which were actual earthquakes, in the same manner as the GAMSEIS events from 2009 to constrain event locations using an appropriate velocity structure.

Some events, especially the events recorded by TAMSEIS in 2002, do not have a good azimuthal coverage in recording stations (Figure 5). To improve the locations, we incorporated polarization information from the recorded Rayleigh waves in the grid search algorithm whenever an accurate polarization direction could be determined. Rayleigh waves have a retrograde elliptical polarization in the radial plane (the vertical plane including the source and receiver), so that polarization measurements provide information on the direction of the event origin from each station. We determined the azimuth of the origin from the station with a 180° ambiguity using the polarization of the two horizontal components, determined using eigenvalue decomposition of the correlation matrix [*Montalbetti and Kanasewich*, 1970]. Then we rotated the waveform into the polarization plane and plot the particle motion of the Rayleigh wave; a retrograde elliptical particle motion indicates the correct direction.

The final locations were determined by minimizing the combined misfit function:

$$E = \sum_{i=1}^{n} \frac{(\text{obsered arrival}_i - \text{predicted arrival}_i)^2}{\text{arrival time } \sigma_i^2} + \sum_{i=1}^{n} \frac{(\text{observed azimuth}_i - \text{predicted azimuth}_i)^2}{\text{azimuth } \sigma_i^2} \quad (1)$$

Traveltime picks and polarization directions were each assigned a quality rating (A, B, and C) and average standard deviation values were assigned for each quality. Arrival picks of quality "A" an arrival time standard deviation of 1.41 s, "B" quality events were assigned 2.24 s, and "C" quality events were assigned 4.0 s. Similarly, we assigned polarization standard deviations: A quality polarization directions an azimuth standard deviation of 4°, B quality of 8°, and C quality of 16°. The estimated azimuth standard deviations are large enough that the solutions are more dependent on arrival times, unless the arrival times fail to adequately constrain the location. The best recorded events show small errors in both arrival time (average misfit for high quality picks is less than 2 s) and polarization direction (average misfit for high quality polarization directions is less than 10°), whereas smaller events with fewer observations and poor signal-to-noise ratios tend to show larger errors.

3.2. Cross-Correlation Scanner Detection

After locating events initially detected by the GAMSEIS seismicity studies, we identified additional firnquakes having similar waveforms using a single channel cross-correlation scanner [*Stankova et al.,* 2008]. We used the waveform recorded at the nearest station from each located event as a correlation detector template and scanned the rest of the recordings from that station for further events. Using the 26 March 2009 event recorded at the nearby station P124 as the template waveform yielded nine additional events large enough to be recorded on more than three stations, and many events recorded on only two stations. Using the other events as templates did not yield any additional events at a reasonable cross-correlation level. The additional nine larger events were then located using the methods described above. Table 1 lists all events with well-constrained locations.

3.3. Jackknife Location Uncertainty Estimation

We tested the robustness of our final locations by applying a jackknife estimate of variance [*Efron and Stein*, 1981]. The jackknife is a simple calculation to help us evaluate the consistency of our solutions and provide an

Table 1. Event Information

Date (Month/Day/Year)	Julian Day	Origin Time	Latitude (deg)	Longitude (deg)	Uncertainty 1σ (km)	Number Arrivals	Number Azimuths	M_L (Median)
01/28/2009	028	01:25:42	−78.80	73.82	2.08	9	9	1.11
03/26/2009	085	09:08:32	−78.79	73.79	11.13	13	10	2.30
03/31/2009	090	18:45:42	−80.29	54.30	27.72	19	18	2.38
04/05/2009	095	07:25:32	−77.60	73.77	39.04	7	5	1.70
04/17/2009	107	11:18:53	−79.89	74.27	66.68	7	6	1.99
04/21/2009	111	06:16:29	−78.69	74.00	2.67	11	8	1.55
04/27/2009	117	10:36:52	−82.43	72.38	96.05	8	5	1.45
05/09/2009	129	06:27:16	−78.57	76.22	8.99	4	4	1.41
06/10/2009	161	08:29:26	−78.66	71.37	4.85	5	5	1.29
07/09/2009	190	02:40:04	−78.82	73.76	5.87	6	6	1.20
07/12/2009	193	15:43:35	−84.93	129.62	30.63	13	11	2.92
08/05/2009	217	04:31:01	−81.37	84.53	71.31	10	4	1.71
08/17/2009	229	18:39:28	−78.09	70.24	6.17	7	5	1.44
10/05/2009	278	00:56:17	−78.76	71.37	9.58	6	4	1.62
10/30/2009	303	13:27:36	−78.10	72.65	16.00	5	5	1.55
11/04/2009	308	00:12:19	−78.35	72.64	3.84	5	5	1.41
11/30/2009	334	00:10:32	−78.84	73.99	10.51	8	7	1.36
12/19/2009	353	02:25:23	−78.81	73.76	2.94	9	8	1.40
01/28/2002	028	08:30:24	−82.72	131.47	2.97	6	6	1.78
01/30/2002	030	09:18:02	−79.93	128.04	4.89	5	5	1.49
01/30/2002	030	19:31:02	−82.02	130.75	2.26	6	5	1.57
01/31/2002	031	06:15:09	−82.03	132.19	<2	6	4	1.46
01/31/2002	031	14:05:44	−81.68	131.47	16.93	5	5	1.24
01/31/2002	031	18:15:19	−81.76	131.12	8.23	5	5	1.52
02/01/2002	032	08:06:42	−81.76	130.42	5.59	5	5	1.41
03/03/2002	034	17:30:29	−80.29	133.84	11.13	5	3	0.39
03/04/2002	035	11:00:25	−82.20	130.73	3.75	5	5	1.58
03/06/2002	037	08:49:56	−81.85	131.47	3.02	5	5	1.52
03/08/2002	039	10:26:53	−82.02	130.75	<2	7	6	1.67

estimate of the standard deviation of the location parameters. The jackknife algorithm involves systematically removing one observation from the grid search input and rerunning the search on the abbreviated data set. After running the search with each observation removed we then calculated the distance between the location with all observations and each location with a single observation removed ($S_{(i)}$). We followed the calculations of *Efron and Stein* [1981] to calculate the variance and standard deviation for the population of solutions:

$$\sigma^2 = \frac{n-1}{n}\sum_{i=1}^{n}\left[S_{(i)} - S_{(\cdot)}\right]^2 \tag{2}$$

where

$$S_{(\cdot)} = \sum_{i=1}^{n}\frac{S_{(i)}}{n} \tag{3}$$

We report the 1σ standard deviation (square root of the variance) in kilometers in Table 1.

3.4. Magnitude Calculation

We calculated a local magnitude (M_L) for each event by determining the median of the magnitudes calculated for each individual observation. The local magnitude is given by [*Stein and Wysession*, 2003]:

$$M_L = \log\frac{A}{T} + 2.76\log Dist - 2.48 \tag{4}$$

where A is the amplitude in microns of the waveforms sampled at period T (we use $T = 1$ s making the first term simply $\log A$) and $Dist$ is the distance (in km) between source and receiver. Magnitudes are given for each event in Table 1.

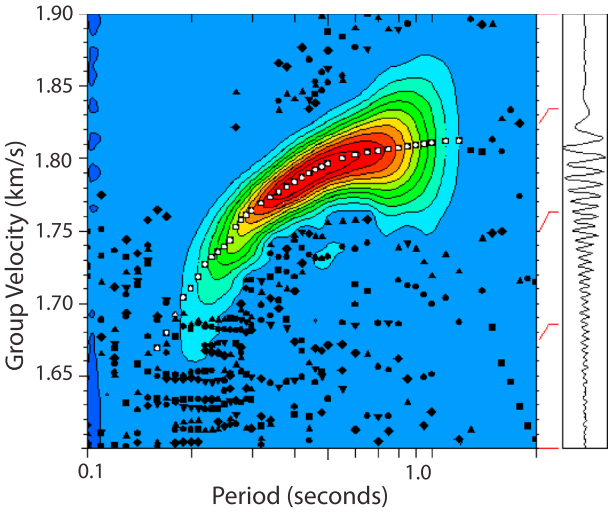

Figure 6. Example of processing window for multiple-filter technique (MFT) analysis [*Herrmann*, 2013] for the 26 March 2009 event recorded at station GM05. Colors and contours represent spectral amplitude; hot colors are highest amplitude. Black symbols represent local peak spectral values after a 2-D search over group velocity/period grid, with square symbols representing the highest peaks. White symbols are selected dispersion values.

3.5. Rayleigh Wave Dispersion Analysis

Analysis of the group velocity dispersion of the Rayleigh wave trains can help us further understand the waveforms and may place important constraints on the ice velocity structure between the source and receiver. To achieve this aim, we performed multiple-filter technique (MFT) analysis [*Dziewonski et al.,* 1969] on the vertical component waveform for several well-recorded events (Figure 6). In total we ran MFT analysis on 57 station/event pairs, some of the best examples are shown in Figures 6 and 7. The MFT calculates a group velocity dispersion curve of the observed seismic wave for a source with known distance [*Herrmann*, 2013]. A narrow band-pass Gaussian filter is applied to the data around a series of center frequencies, and the time axis is converted to velocity. The maximum of the envelope of the filtered signal corresponds to the velocity of the group velocity arrival at each frequency [*Herrmann*, 2013].

We inverted the resulting dispersion curve to determine the best shear velocity structure using partial derivatives calculated by frequency-wave number integration (Figure 7). Following *Herrmann* [2013], we ran an iterative linearized inversion beginning with a starting input model until the calculated velocity approximated the observed data. The inversion calculates the misfit between the observed data and the current model (starting with the initial input model) and adjusts the model with each iteration to reduce misfit. The procedure requires that layer thicknesses be specified a priori, so layer thicknesses must be chosen to provide reasonable resolution, which can be checked using the resolution matrix of the inversion. If many thin layers are used there is significant trade-off between layers and very little velocity resolution in the individual layers [*Douma and Haney*, 2013], we therefore adopt a model utilizing 50 m thick upper layers and progressively thicker layers with depth (Table 2). The best fitting models retain some trade-off in the upper 2–3 layers, as indicated by the resolution matrices (Figures 7d and 7h).

The starting model for the velocity inversion was based on a study by *Albert* [1998] of the seismic velocity and density of ice in a borehole 10 km from the South Pole (Table 2). South Pole is located on the interior of the East Antarctic ice sheet a few hundred kilometers from the GAMSEIS array, with roughly similar temperature conditions and so represents a reasonable approximation to the ice sheet in the study region. Average values for glacial ice [*Albert*, 1998] were used for depths greater than 200 m. Velocities were inverted using both an ice half-space and a model with ice over a rock half-space. However, as the Rayleigh wave eigenfunctions are entirely in the ice layer for the observed frequencies and East Antarctic ice thicknesses, our final models use ice velocities for the half-space and do not contain a rock layer. The dispersion curves are able to fit the data very well for most of the stations (Figures 7c and 7g). We used only the well-fit data in our further investigations and modeling.

3.6. Reflectivity Synthetic Calculations

We modeled the waveforms associated with several station event pairings following the reflectivity methods of *Kennett* [2001] in order to constrain the source depth. This method calculates the complete seismic response for a specified moment tensor source mechanism and a given 1-D velocity, density, and *Q* structure. We estimated a Q_P of 200–400 and a Q_S of 90–180 for Antarctic ice based on values reported in various studies [*Gusmeroli et al.,* 2010; *Peters et al.,* 2012]. We compared several different velocity and density structure

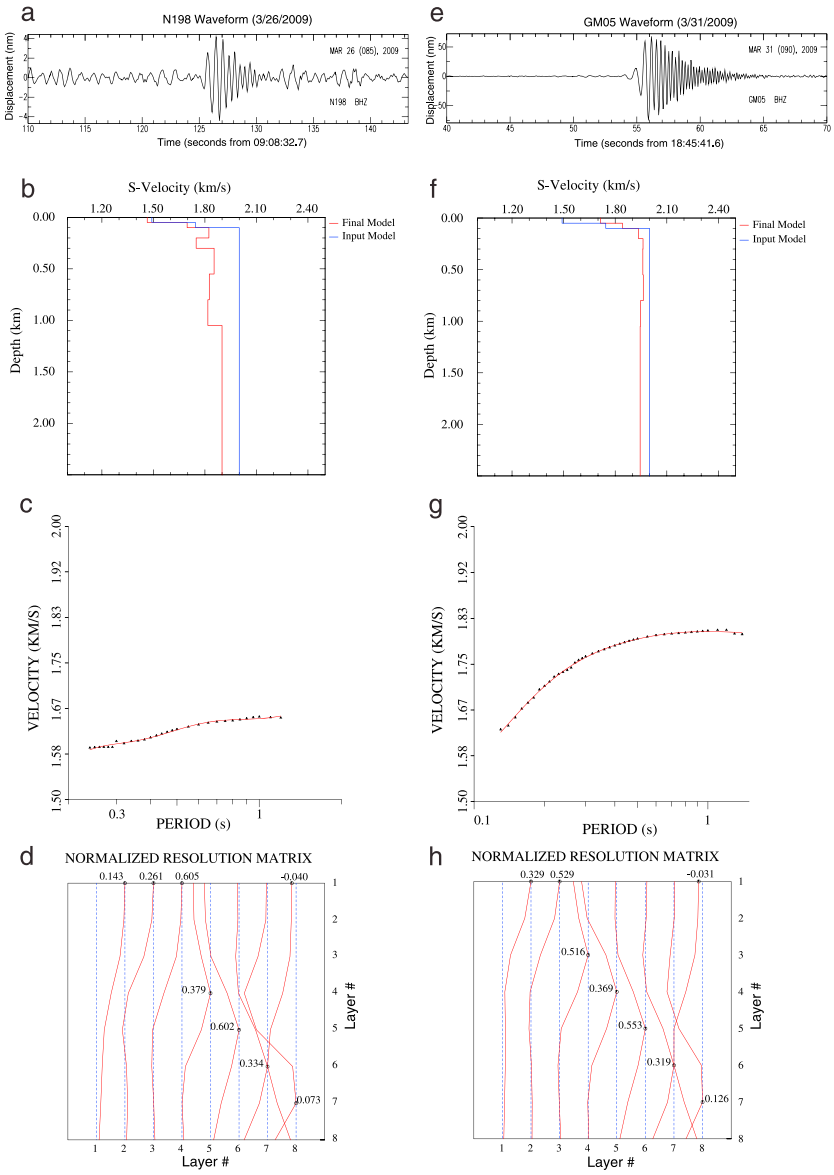

Figure 7. Examples of inverting the observed dispersion curves for shear velocity structure for two station/event pairs. (a) Waveform for event on 26 March 2009 recorded at station N198 (203 km distance). Time scale on the *x* axis is relative to the event origin time. (b) The input model (blue) and final *s* velocity inversion model (red). (c) The fit of the calculated dispersion curve (line) to the data (triangles). (d) The resolution matrix for the *s* velocity inversion, indicating that the top three layers and the bottom half-space layer are not independently resolved. (e) Waveform for event on 31 March 2009 recorded at station GM05 (116 km distance). (f) The input model (blue) and final *s* velocity inversion model (red). (g) The fit of the calculated dispersion curve (line) to the data (triangles). (h) The resolution matrix for the *s* velocity inversion, indicating that the top two layers and the bottom half-space layer are not independently resolved.

inputs. The first model was adapted from *Albert* [1998] for all ice layers with preliminary reference Earth model for underlying rock layers. We also tested structures taken directly from the MFT dispersion curve inversions. Most structures from the dispersion curve inversion show one or more slight low-velocity zones, we additionally modified such structures to only allow velocity to increase with depth. The final model for the 26 March 2009 event recorded at station P116 is shown in Table 3, with upper crustal layers from a global velocity model added.

Although the general arrival times and characteristics of the waveforms can be well fit, the complex, high-frequency nature of the dispersed arrivals, and the deviation of the actual ice structure from the path average 1-D structure used here prevent an exact match between the observed and calculated waveforms. Thus, we

Table 2. Starting Model for *S* velocity Inversion[a]

Depth (m)	*P* Velocity (km/s)	*S* Velocity (km/s)	Density (g/cm^3)
0	2.909	1.491	0.691
50	3.382	1.745	0.800
100	3.927	2.000	0.945
200	3.927	2.000	0.945
300	3.927	2.000	0.945
550	3.927	2.000	0.945
800	3.927	2.000	0.945
½ Space	3.927	2.000	0.945

[a]Depths denote the depth of the top of constant velocity layers.

computed the envelope function of both the observed and the synthetic waveforms and compared the amplitudes. To evaluate the likely source depth, we computed reflectivity synthetic waveforms for hypothetical sources at different depths (from the ice surface to middle-to-lower ice layers) and compared them to the observed seismograms (Figure 8). These tests were done for a variety of possible moment tensors including strike-slip and dip-slip double couple sources as well as implosion sources in order to ascertain if there is a significant difference in the amplitudes of surface and body waves with variation in source mechanism.

4. Results

4.1. Locations

We locate events in two general areas controlled by the location of the individual arrays. There are 18 events recorded by enough stations to be well located in 2009 (Table 1), with all events occurring within the confines of the GAMSEIS array (Figure 4). Table 1 lists only the events large enough to be observed on multiple stations. Many events detected by the cross-correlation scanner in the vicinity of station P124 (Figure 4) are too small to be observed on additional instruments and therefore cannot be located. Event magnitudes range between M_L 1.11 and 2.92, with an average magnitude of M_L 1.66. Many of the event epicenters are well constrained, with jackknife uncertainties of less than 10 km.

The events occurring in 2002 are closely grouped about 400 km from the TAM and within 300 km of the TAMSEIS stations (Figure 5). These events are typically smaller than the events recorded in 2009 (see M_L column in Table 1), are detected at closer distances to the stations, and the duration of the dispersed signal is slightly shorter (Figure 2b versus Figure 2a). Event magnitudes range from M_L 0.39–1.78 with an average magnitude of M_L 1.42. Table 1 lists only the events that were recorded by enough stations to obtain well-constrained locations, but many more small events were recorded on one or two stations. The number of events per day in 2002 varies greatly and shows some characteristics of swarms, on some days as many as 10 events can be observed while on other days no events are detected. Unfortunately, the recording stations form a linear array except for one station which is slightly offline (Figures 1 and 5), which frequently gives two possible locations, one on each side of the line. Due to this station configuration we use the polarization direction and the retrograde particle motion of the recorded Rayleigh waveforms to better constrain event locations.

Table 3. Structure Model From Inversion of the 26 March 2009 Event Recorded at Station P116 and Used for Reflectivity Synthetic Modeling[a]

Depth (km)	*P* Velocity (km/s)	*S* Velocity (km/s)	Density (g/cm^3)	Q_p	Q_s
0.00	1.974	1.011	0.456	200	90
0.05	2.736	1.412	0.638	200	90
0.10	3.415	1.740	0.796	400	180
0.20	3.416	1.740	0.796	400	180
0.30	3.537	1.800	0.824	400	180
0.55	3.550	1.807	0.827	400	180
0.80	3.560	1.813	0.830	400	180
1.05	3.747	1.905	0.873	400	180
2.60	5.814	3.208	2.594	1350	600
15.02	6.816	3.909	2.893	1350	600

[a]Depths denote the depth of the top of constant velocity layers.

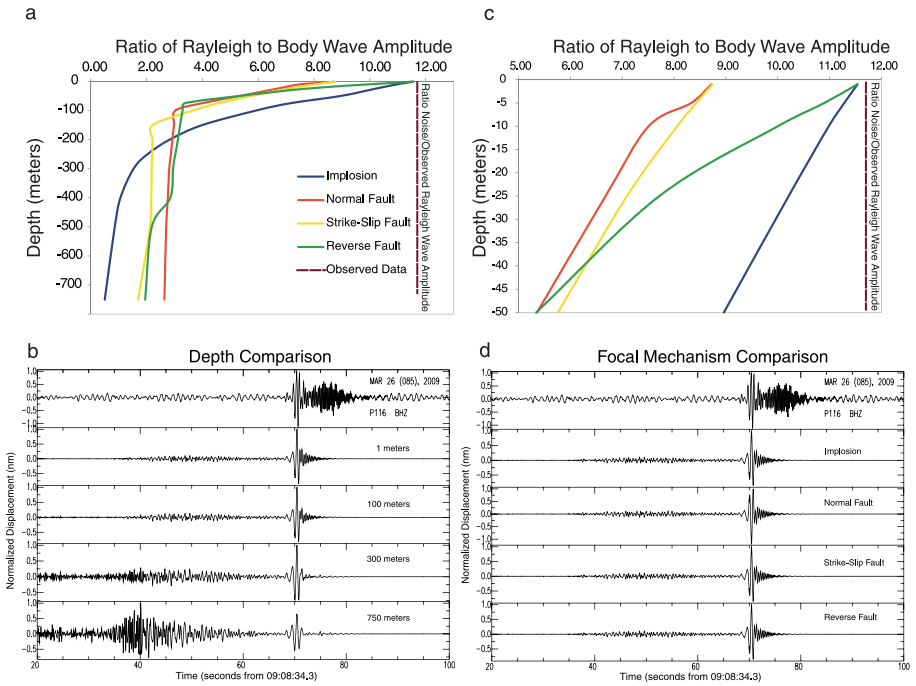

Figure 8. Depth determination from synthetic modeling. (a) Plot of the ratio of maximum Rayleigh wave to maximum body wave amplitude for the 26 March 2009 event recorded at station P116 (113 km distance) compared to the same ratios for synthetics. The observed ratio between Rayleigh wave amplitude and the background noise level is 11.7, as indicated by the dotted red line. Synthetics consistent with the data should be near or above this ratio. Other lines show the ratio of synthetic Rayleigh to body wave amplitudes with increasing depth for four source types. The ratio of synthetic Rayleigh wave to body wave amplitude approach the ratio of observed Rayleigh wave to noise for the shallowest sources ($h < 50$ m). (b) Observed data and synthetics calculated for various source depths for the same event and station used in Figure 8a. Waveforms are vertical component with a 0.9–5 Hz band-pass filter applied, normalized to maximum value. An implosion source is used to generate synthetics. Times on the *x* axis are relative to the event origin time. (c) Detail of upper 50 m of Figure 8a. (d) Observed data and synthetic waveforms calculated for various source types at 50 m source depth for same event and station used in Figure 8a. Waveforms are vertical component with a 0.9–5 Hz band-pass filter applied, normalized to maximum value.

4.2. Rayleigh Wave Dispersion Results

The dispersion analysis generally results in models that show an increase in shear velocity with depth. Velocity typically increases from 1.2 to 1.4 km/s in the upper 50 m to around 1.8 km/s by 100–200 m depth and then remains fairly constant through the rest of the ice layers. Even slower velocities are likely present in the upper few meters of the firn but cannot be resolved with this data. We find variation in the velocity dispersion between events and even between stations in a single event. This is to be expected as the individual station/event pairings reflect the unique path traveled. As the thickness of the firn layer and therefore overall compaction of the upper layers is variable, we should anticipate lateral variations in the shallow velocity structure. Small variations in the determined velocities may also result from uncertainties in the event locations. The largest frequency range we observe is from approximately 0.8 Hz to 10 Hz (Figure 7), but in most cases a narrower range of frequencies is visible above the noise level.

The dispersion analysis demonstrates that the observed waveforms are compatible with the known shear velocity structure of the ice sheet, and also shows that there are regional variations. The results suggest that the low-velocity firn layer of East Antarctica varies in thickness from a minimum of 100 m up to a maximum of 200 m (Figures 7b and 7f). Our findings agree with the results from *van den Broeke* [2008] showing that the firn layer in East Antarctica is slightly more than 100 m. We can also see from the results that shear velocity is laterally variable (compare Figure 7b to Figure 7f).

4.3. Reflectivity Synthetic Modeling

One conspicuous characteristic of the observed waveforms is the complete absence of body wave arrivals observable above the noise level, as the signals are dominated by the surface waves. We attempt to replicate

this observation with the synthetic seismograms and thereby use it to help constrain the source depth. We compare the amplitudes of body and Rayleigh waves observed in the modeled waveforms to those recorded in the observed vertical component noise and Rayleigh wave for several stations recording our largest events (Figure 8). The amplitude of the noise in the observed seismogram represents the largest possible body wave arrival, and thus the ratio of Rayleigh wave to noise amplitude represents a lower bound on the observed Rayleigh wave to body wave amplitude ratio. The Rayleigh wave to body wave amplitude ratio decreases with increasing source depth for the synthetic seismograms (Figures 8a and 8b). Therefore, in order for a source depth to be appropriate, the ratio of Rayleigh wave to body wave amplitude in the synthetic must be greater than the ratio of Rayleigh wave to noise amplitude in the observed waveforms (Figure 8a). Only synthetic seismograms for the shallowest source depths, at depths less than about 20 m, match the failure to visually observe body wave arrivals above the noise level on the records, suggesting that the source depth must be extremely shallow.

We generate synthetic waveforms for several generic faults including dip-slip (both normal and reverse), strike-slip, and implosion (explosion sources produce the same waveform as implosion source with opposite polarity). Additional double couple sources are tested for a variety of fault strikes, dips, and slips. We also test the moment tensor for a Mode I tensile crack opening which is essentially a combination of a compensated linear vector dipole source and an implosion/explosion source [*Stein and Wysession*, 2003]. All tested source mechanisms show observable body waves and decreases in the ratio of Rayleigh wave to body wave amplitude with depth further supporting our conclusion of a very shallow source (Figures 8a and 8c). We investigate a variety of depths (1 m, 5 m, 10 m, 25 m, 50 m, 75 m, 100 m, 150 m, 200 m, 250 m, 300 m, 400 m, 500 m, and 750 m) for our best station/event pairings. We then calculate the ratio of the amplitude of Rayleigh wave to body wave for each depth (Figure 8a). The ratio decreases with increased depth for all mechanism types, and only for the shallowest depths (10–20 m) do the synthetic ratios approach the observed ratio of Rayleigh wave to background noise. For a given focal mechanism we can see that increases in source depth produce corresponding increases in body wave amplitudes relative to surface wave amplitudes. By 750 m, body wave amplitudes are larger than associated Rayleigh wave amplitudes (Figure 8b). Synthetics calculated with different source mechanism types are relatively similar for these shallow source depths suggesting that variations in the body/Rayleigh wave amplitudes are controlled by source depth (Figure 8c). From these tests we estimate the depths of the events to be in the upper 10–20 m of the firn layer.

5. Discussion

5.1. Event Characteristics and Locations

We locate 18 events on the East Antarctic Plateau and 11 events close to the TAM, most of them with a 1σ uncertainty less than 15 km (Figures 1, 4, and 5). These events are small (M_L 0.39–2.92) but much larger than crevassing events recorded in other glacial settings [e.g., *Walter et al.,* 2009], and the events are recorded to much larger distances than typical crevasse-related icequakes. The event waveforms show no visually observable body waves, unlike crevassing events observed on smaller glaciers at closer distances [*Neave and Savage*, 1970; *Walter et al.,* 2009]. These characteristics indicate we are likely looking at a previously unreported type of icequake. Alternatively, these events may simply be larger icequakes occurring in a novel environment, on the interior of a continental ice sheet, resulting in unique waveforms.

Temporal seismicity variations such as diurnal or seasonal patterns can provide important constraints on the causative mechanism and have been reported for icequakes on Mount Erebus, where they are attributed to temperature variations in the uppermost firn layer [*Rowe et al.,* 2005]. The 2002 data set is limited to 3 months in the late Austral summer, so is of limited usefulness. However, the 2009 data set extends throughout an entire year, so should provide some information on seasonality. The 2009 firnquakes occurred throughout the year in all weather and solar conditions. The only months with no firnquakes were February and September. There is some evidence for a seasonal pattern, as the highest activity rate occurs from 26 March to 9 May, when 7 out of the 18 events occur within a 45 day period. This time period corresponds to the onset of the polar winter, so may indicate some connection to seasonal temperature cycles, but a larger data set will be necessary to confirm this hypothesis.

There are two areas of high event density. A majority of events from 2009 are located to the geographic northwest of station P124 as the ice slopes downward toward the Lambert Graben (Figure 4) and most events

from 2002 are also closely grouped to the south of station N084 (Figure 5). Both of these areas have a dense population of wind-glazed crevasses and steeper surface slopes [*Byers et al.,* 2013; L. C. Byers et al., manuscript in preparation, 2015]. It also should be noted that events in these two areas at times exhibit swarm-like behavior, although most of the events during swarm periods are too small to be located with a high degree of accuracy and as such are not reported in Table 1 or shown in our figures. Several events are scattered beyond the densely crevassed areas, especially within the GAMSEIS array, but all of these events appear to be isolated, at least within our study period. Areas of multiple firnquakes seem to correlate well with areas of high crevasse density. There are no similar firnquakes found in a seismicity study of West Antarctica [*Lough*, 2014], where there are no reported wind-glazed crevasses. This study has similar station coverage and event detection capability to the GAMSEIS array and so should readily record firnquakes if they are present. Thus, we conclude that firnquakes occur much more frequently in East Antarctica, or may be unique to the region.

5.2. Source Depths

The synthetic modeling leads to one main conclusion: the source must be located in the upper 10–20 m of ice. Such a shallow depth (consistent with the depths assumed in other crevasse seismicity studies such as *Neave and Savage* [1970]; *Chichowicz* [1983]; and *Walter et al.* [2009]) necessitates a source near the top of the firn layer and precludes the possibility of either a basal or midice source. We further conclude that our claim that the source must be located in the upper 10–20 m of firn is robust, even if a wide variety of source mechanisms are considered (Figures 8a and 8c). This depth suggests that the firnquakes may likely have a surface expression at the top of the firn layer that could be observed in satellite photos.

5.3. Interpretation in Terms of Ice Sheet Processes

The observations here provide important constraints on the causative process of the firnquakes. We initially considered the possibility that the firnquake waveforms resulted from a phenomenon sometimes previously referred to as firnquakes but more often termed whumpfs [*Sorge*, 1933; *Den Hartog*, 1982; *Johnson et al.,* 2005; *Heierli*, 2005]. Whumpfs consist of sudden firn collapse events that may propagate for up to several kilometers. Detailed field observations are lacking but it is suggested the propagation velocities of whumpfs can vary greatly from 6 m/s up to 330 m/s, with total source durations on the order of 10–100 s [*Truman*, 1973; *Den Hartog*, 1982; *Heierli*, 2005]. Since the waveforms observed here show frequencies ranging from 1 to 10 Hz they must involve source durations on the order of a second or less, thus making it unlikely that the waveforms result from the long-duration whumpfs previously reported. In addition, most of the sources described here show Love waves and are thus inconsistent with isotropic or vertical single-force sources, which are the likely source mechanisms for whumpfs. Another inconsistency between whumpfs and firnquakes is that whumpfs are most often reported as individual events while the events reported here have shown swarm-like behavior [*Sorge*, 1933; *Den Hartog*, 1982; *Johnson et al.,* 2005; *Heierli*, 2005]. While we are not able to completely rule out the possibility that whumpfs produce the observed firnquake waveforms, the previously described characteristics of whumpfs as well as the spatial association of firnquakes with crevasse fields suggest a crevasse source instead.

Most of the shallowest icequakes previously studied in other environments are associated with traditional crevasse formation [*Neave and Savage*, 1970; *Walter et al.,* 2009]. In alpine glaciers, where most previous crevasse seismicity studies have focused, crevassing often affects only the uppermost 20 m or so of ice [*Walter et al.,* 2009]. However, the East Antarctic Ice Sheet is many times thicker than the alpine glaciers previously studied and flowing under completely different velocity, slope, and bed conditions producing a completely different strain regime so there is no reason to expect identical behavior in crevasse formation. The icequakes reported here should therefore be expected to show variation in characteristics when compared to previously reported seismicity associated with crevassing.

We investigated the possibility that firnquakes are associated with ice deformation features on the surface, such as large-scale crevasse fields, especially those that border ice streams and form where ice flows over large changes in topography. No such features are visible on Landsat Image Mosaic of Antarctica satellite imagery of the event locations. In addition, velocity maps show the events all occur in regions of low surface ice velocity and low strain rate [*Rignot et al.,* 2011]. However, many events coincide with mapped small-scale surface crevasses located on wind-glazed ice surfaces (Figures 1, 4, and 5) [*Byers et al.,* 2013]. Both the 2002 and the 2009 data sets show many of the events clustered spatially in close proximity to a concentration of

small crevasses (Figures 4 and 5). The correlation between small-scale surface crevasses and seismic events suggests the two are linked, and this is consistent with the observed very shallow source depth. It is also interesting to note that neither do we observe any firnquakes in West Antarctica nor have any been reported to date, and no wind-glazed crevasse features have yet been identified in West Antarctica [*Byers et al.,* 2013]. We therefore expect that firnquakes are rare or absent in West Antarctica as wind-glazed crevasse features have not been identified there.

Byers et al. [2013] interpreted the wind-glazed crevasse features as the result of tension imposed on randomly oriented preexisting cracks within the wind-glazed surface. They are smaller features than traditional crevasses located on the margins of ice streams or associated with large changes in glacier elevation. Wind-glazed surfaces, denoted by their polished appearance, are found on the leeward slopes of ice sheet undulations and megadunes in areas of near-zero net surface accumulation resulting from persistent katabatic winds [*Scambos et al.,* 2012]. Vertical cracks, termed "macrocracks," have been observed at many areas on the plateau most likely linked to areas of low net surface accumulation (such as wind-glazed surfaces) [*Severinghaus et al*., 2010]. Macrocracks can enlarge due to sublimation and potentially form the observed wind-glazed crevasses. Macrocracks are small compared to many types of crevasses, only about 10 cm wide and are thought to form as a result of thermal contraction during the winter when snow that is sufficiently hardened can support the buildup of tensile stress and eventually fracture [*Severinghaus et al.,* 2010; *Byers et al.,* 2013]. The high rate of firnquake activity at the onset of the Antarctic winter during March through May is consistent with a thermal contraction origin for many of the events. The shallow depth of the firnquakes is also consistent with their association to the shallow macrocracks, which are thought to aid air circulation through the East Antarctic firn layer up to a depth of 23 m [*Severinghaus et al.,* 2010]. Although still subject to confirmation, a compelling case can be made for associating the firnquakes with the formation and enlargement of contraction cracks near the surface of the ice sheet in wind-glazed terrains.

6. Conclusions

We report a previously undocumented type of seismic source in the upper snow layers of the East Antarctic Ice Sheet that we denote as firnquakes. We detected events in two different field deployments on the East Antarctic interior: the 2009 GAMSEIS deployment and the 2002 TAMSEIS deployment. The seismic signals are measurable at distances of nearly 1000 km and are characterized by dispersed 1–10 Hz Rayleigh waves, with no observable presence of direct *P* and *S* arrivals. Analysis of the Rayleigh wave dispersion yields shear wave velocity structures that are compatible with shear velocity structures known from ice cores. These results demonstrate that the waveforms represent Rayleigh waves propagating entirely within the ice sheet. Waveform modeling shows that these arrivals must have been generated by sources within the firn layer, and probably in the upper 20 m. Due to the shallow event hypocenters and correlation to mapped crevasse locations, we propose they are most likely associated with crevassing in regions of persistent katabatic winds and surface glazing. Future follow-on studies of the source moment tensors may yield further insight into the physical processes causing these events.

Acknowledgments

Data used in this study were collected as part of the GAMSEIS and TAMSEIS deployments and is available via the IRIS data management center (http://ds.iris.edu/ds/nodes/dmc). We would like to thank all members of the GAMSEIS and TAMSEIS field teams who collected the data used here as well as the IRIS data management center for maintaining the archived data. Instruments for both experiments were provided by IRIS/PASSCAL instrument center in Socorro, NM. We also want to thank Dan Bartz and Zihe Zhang for their work on initial identification of potential events. This work has been supported by National Science Foundation grants ANT-0537597, ANT-0838934, and PLR-1246712.

References

Albert, D. G. (1998), Theoretical modeling of seismic noise propagation in firn at the South Pole, Antarctica, *Geophys. Res. Lett.*, *25*(23), 4257–4260, doi:10.1029/1998GL900155.

Allstadt, K., and S. Malone (2014), Swarms of stick-slip icequakes triggered by snow loading at Mount Rainier volcano, *J. Geophys. Res. Earth Surf.*, *119*, 1180–1203, doi:10.1002/2014JF003086.

Anandakrishnan, S., and C. R. Bentley (1993), Micro-earthquakes beneath Ice Streams B and C, West Antarctica: Observations and implications, *J. Glaciol.*, *39*, 455–462.

Bannister, S., and B. L. N. Kennett (2002), Seismic activity in the Transantarctic Mountains-Results from a broadband array deployment, *Terra Antarct.*, *9*(1), 41–46.

Barklage, M., D. A. Wiens, A. Nyblade, and S. Anandakrishnan (2009), Upper mantle seismic anisotropy of South Victoria Land and the Ross Sea coast, Antarctica from SKS and SKKS splitting analysis, *Geophys. J. Int.*, *178*(2), 729–741, doi:10.1111/j.1365-246X.2009.04158.x.

Bartholomaus, T. C., C. F. Larsen, S. O'Neel, and M. E. West (2012), Calving seismicity from iceberg-sea surface interactions, *J. Geophys. Res.*, *117*, F04029, doi:10.1029/2012JF002513.

Byers, L. C., L. A. Stearns, and C. J. van der Veen (2013), Crevasses forming in wind-glazed surfaces of East Antarctica, 2013 WAIS Workshop, Sterling, Va.

Canassy, P. D., J. Faillettaz, F. Walter, and M. Huss (2012), Seismic activity and surface motion of a steep temperate glacier: A study on Triftgletscher, Switerland, *J. Glaciol.*, *58*(209), 513–528, doi:10.3189/2012JoG11J104.

Caplan-Auerbach, J., and C. Huggel (2007), Precursory seismicity associated with frequent, large ice avalanches on Iliamna volcano, Alaska, USA, *J. Glaciol.*, *53*(180), 128–140.

Carmichael, J. D., E. C. Pettit, M. Hoffman, A. Fountain, and B. Hallet (2012), Seismic multiplet response triggered by melt at Blood Falls, Taylor Glacier, Antarctica, *J. Geophys. Res.*, *117*, F03004, doi:10.1029/2011JF002221.

Carmichael, J. D., I. Joughin, M. D. Behn, S. Das, M. A. King, L. Stevens, and D. Lizarralde (2015), Seismicity on the western Greenland Ice Sheet: Surface fracture in the vicinity of active moulins, *J. Geophys. Res. Earth Surf.*, *120*, 1082–1106, doi:10.1002/2014JF003398.

Chen, X., P. M. Shearer, F. Walter, and H. A. Fricker (2011), Seventeen Antarctic seismic events detected by global surface waves and a possible link to calving events from satellite images, *J. Geophys. Res.*, *116*, B06311, doi:10.1029/2011JB008262.

Chichowicz, A. (1983), Icequakes and glacier motion: The Hans Glacier, Spitsbergen, *Pure Appl. Geophys.*, *121*(1), 27–38.

Danesi, S., S. Bannister, and A. Morelli (2007), Repeating earthquakes from a rupture of an asperity under an Antarctic outlet glacier, *Earth Planet. Sci. Lett.*, *253*(1–2), 151–158, doi:10.1016/j.epsl.2006.10.023.

Den Hartog, S. L. (1982), Firn quake: A rare and poorly explained phenomenon, *Cold Reg. Sci. Technol.*, *6*, 173–174.

Douma, H., and M. M. Haney (2013), Exploring nonlinearity and nonuniqueness in surface-wave inversion for near-surface velocity estimation, *Leading Edge*, *32*(6), 648–655, doi:10.1190/tle32060648.1.

Dziewonski, A., S. Bloch, and M. L. Landisman (1969), A technique for the analysis of transient seismic signals, *Bull. Seismol. Soc. Am.*, *59*(1), 427–444.

Efron, E. F., and C. Stein (1981), The jackknife estimate of variance, *Ann. Stat.*, *9*(3), 586–596.

Ekström, G., M. Nettles, and G. A. Abers (2003), Glacial earthquakes, *Science*, *302*(5645), 622–624, doi:10.1126/science.1088057.

Gusmeroli, A., R. A. Clark, T. Murray, A. D. Booth, B. Kulessa, and B. E. Barrett (2010), Seismic wave attenuation in the uppermost glacier ice of Storglaciaren, Sweden, *J. Glaciol.*, *56*(196), 249–256.

Hansen, S. E., A. A. Nyblade, D. S. Heeszel, D. A. Wiens, P. Shore, and M. Kanao (2010), Crustal structure of the Gamburtsev Mountains, East Antarctica, from S-wave receiver functions and Rayleigh wave phase velocities, *Earth Planet. Sci. Lett.*, *300*, 395–401, doi:10.1016/j.epsl.2010.10.022.

Harvey, D. J. (2003), Antelope: A software infrastructure for the support of virtual observatories, AGU Fall Meeting Abstracts, Abstract U22A-0009.

Heeszel, D. S., D. A. Wiens, A. A. Nyblade, S. E. Hansen, M. Kanao, M. An, and Y. Zhao (2013), Rayleigh wave constraints on the structure and tectonic history of the Gamburtsev Subglacial Mountains, East Antarctica, *J. Geophys. Res. Earth Surf.*, *118*, 2138–2153, doi:10.1002/jgrb.50171.

Heeszel, D. S., H. A. Fricker, J. N. Bassis, S. O'Neel, and F. Walter (2014), Seismicity within a propagating ice shelf rift: The relationship between icequake locations and ice shelf structure, *J. Geophys. Res. Earth Surf.*, *119*, 731–744, doi:10.1002/2013JF002849.

Heierli, J. (2005), Solitary fracture waves in metastable snow stratifications, *J. Geophys. Res.*, *110*, F02008, doi:10.1029/2004JF000178.

Herrmann, R. B. (2013), Computer programs in seismology: An evolving tool for instruction and research, *Seismol. Res. Lett.*, *84*(6), 1081–1088, doi:10.1785/0220110096.

Johnson, B. C., J. B. Jamieson, and R. R. Stewart (2005), Seismic measurements of fracture speed in a weak snowpack layer, *Cold Reg. Sci. Technol.*, *40*, 41–45, doi:10.1016/j.coldregions.2004.05.003.

Kennett, B. L. N. (2001), *The Seismic Wavefield: Volume 1. Introduction and Theoretical Development*, 380 pp., Cambridge Univ. Press, Cambridge.

Lough, A. C. (2014), Studies of seismic sources in Antarctica using an extensive deployment of broadband seismographs, PhD thesis, Dept. of Earth and Planet. Sci., Washington Univ., St. Louis, Mo.

Mikesell, T. D., K. van Wijk, M. M. Haney, J. H. Bradford, H. P. Marshall, and J. T. Harper (2012), Monitoring glacier surface seismicity in time and space with Rayleigh waves, *J. Geophys.*, *117*, F02020, doi:10.1029/2011JF002259.

Montalbetti, J. F., and E. R. Kanasewich (1970), Enhancement of teleseismic body phases with a polarization filter, *Geophys. J. Int.*, *21*(2), 119–129, doi:10.1111/j.1365-246X.1970.tb01771.x.

Moore, P. L., J. P. Winberry, N. R. Iverson, K. A. Christianson, S. Anandakrishnan, M. Jackson, M. E. Mathison, and D. Cohen (2013), Glacier slip and seismicity induced by surface melt, *Geology*, *41*(12), 1247–1250, doi:10.1130/G34760.1.

Neave, K. G., and J. C. Savage (1970), Icequakes on the Athabasca Glacier, *J. Geophys. Res.*, *75*(8), 1351–1362, doi:10.1029/JB075i008p01351.

Nettles, M., and G. Ekström (2010), Glacial earthquakes in Greenland and Antarctica, *Annu. Rev. Earth Planet. Sci.*, *38*(1), 467, doi:10.1146/annurev-earth-040809-152414.

Peng, Z., J. I. Walter, R. C. Aster, A. Nyblande, D. A. Wiens, and S. Anandakrishnan (2014), Antarctic icequakes triggered by the 2010 Maule earthquake in Chile, *Nat. Geosci.*, *7*, 677–681, doi:10.1038/NGEO2212.

Peters, L. E., S. Anandakrishnan, R. B. Alley, and D. E. Voigt (2012), Seismic attenuation in glacial ice: A proxy for englacial temperature, *J. Geophys. Res.*, *117*, F02008, doi:10.1029/2011JF002201.

Pratt, M. J., J. P. Winberry, D. A. Wiens, S. Anandakrishnan, and R. B. Alley (2014), Seismic and geodetic evidence for grounding-line control of Whillans Ice Stream stick-slip events, *J. Geophys. Res. Earth Surf.*, *119*, 333–348, doi:10.1002/2013JF002842.

Rignot, E., J. Mouginot, and B. Scheuchl (2011), Ice flow of the Antarctic ice sheet, *Science*, *333*(6048), 1427–1430, doi:10.1126/science.1208336.

Röösli, C., F. Walter, S. Husen, L. C. Andrews, M. P. Lüthi, G. A. Catania, and E. Kissling (2014), Sustained seismic tremors and icequakes detected in the ablation zone of the Greenland ice sheet, *J. Glaciol.*, *60*(221), 563–575, doi:10.3189/2014JoG13J210.

Roux, P.-. F., F. Walter, P. Riesen, S. Sugiyama, and M. Funk (2010), Observation of surface seismic activity changes of an Alpine glacier during a glacier-dammed lake outburst, *J. Geophys. Res.*, *115*, F03014, doi:10.1029/2009JF001535.

Rowe, C. A., R. C. Aster, P. R. Kyle, and A. E. Eschenbacher (2005), Seismic observations at Mount Erebus Volcano Observatory: 1997–1998, *Ant. J. U. S.*, *33*, 335–339.

Scambos, T. A., et al. (2012), Extent of low-accumulation "wind glaze" areas on the East Antarctic plateau: Implications for continental ice mass balance, *J. Glaciol.*, *58*(210), 633–647, doi:10.3189/2012JoG11J232.

Scambos, T., T. Haran, M. Fahnestock, T. Painter, and J. Bohlander (2007), MODIS-based Mosaic of Antarctica (MOA) data sets: Continent-wide surface morphology and snow grain size, *Remote Sens. Environ.*, *111*(2–3), 242–257, doi:10.1016/j.rse.2006.12.020.

Severinghaus, J. P., et al. (2010), Deep air convection in the firn at a zero-accumulation site, central Antarctica, *Earth Planet. Sci. Lett.*, *293*(3), 359–367, doi:10.1016/j.epsl.2010.03.003.

Sorge, E. (1933), The scientific results of the Wegener expeditions to Greenland, *Geophys. J.*, *81*, 333–334.

Stankova, J., S. L. Bilek, C. A. Rowe, and R. C. Aster (2008), Characteristics of the October 2005 microearthquake swarm and reactivation of similar event seismic swarms over decadal time periods near Socorro, New Mexico, *Bull. Seismol. Soc. Am.*, *98*(1), 93–105, doi:10.1785/0120070108.

Stein, S., and M. Wysession (2003), *An Introduction to Seismology, Earthquakes, and Earth Structure*, Blackwell, Malden, Mass.

Thelen, W. A., K. Allstadt, S. De Angelis, S. D. Malone, S. C. Moran, and J. Vidale (2013), Shallow repeating seismic events under an alpine glacier at Mount Rainier, Washington, USA, *J. Glaciol.*, *59*(214), 345–356, doi:10.3189/2013JoG12J111.

Truman, J. C. (1973), Wave propagation in snow, *Am. J. Phys.*, *41*, 282–283.
Tsai, V. C., and G. Ekström (2007), Analysis of glacial earthquakes, *J. Geophys. Res.*, *112*, F03S22, doi:10.1029/2006JF000596.
Tsai, V. C., J. R. Rice, and M. Fahnestock (2008), Possible mechanisms for glacial earthquakes, *J. Geophys. Res.*, *113*, F03014, doi:10.1029/2007JF000944.
van den Broeke, M. (2008), Depth and density of the Antarctic firn layer, *Arct. Antarct. Alp. Res.*, *40*(2), 432–438, doi:10.1657/1523-0430(07-021)[BROEKE]2.0.CO;2.
Walter, F., N. Deichmann, and M. Funk (2008), Basal icequakes during changing subglacial pressures beneath Gornergletscher, Switzerland, *J. Glaciol.*, *54*(186), 511–521, doi:10.3189/002214308785837110.
Walter, F., J. F. Clinton, N. Deichmann, D. S. Dreger, S. E. Minson, and M. Funk (2009), Moment tensor inversions of icequakes on Gornergletscher, Switzerland, *Seismol. Soc. Am. Bull.*, *99*(2A), 852–870, doi:10.1785/0120080110.
Walter, F., D. S. Dreger, J. F. Clinton, M. Deichmann, and M. Funk (2010), Evidence for near-horizontal tensile faulting at the base of Gornergletscher,a Swiss alpine glacier, *Seismol. Soc. Am. Bull.*, *100*(2), 458–472, doi:10.1785/0120090083.
Walter, F., P. Roux, C. Roeoesli, A. Lecointre, D. Kilb, and P. F. Roux (2015), Using glacier seismicity for phase velocity measurements and Green's function retrieveal, *Geophys. J. Int.*, *201*, 1722–1737, doi:10.1093/gji/ggv069.
Walter, F., J. M. Amundson, S. O'Neel, M. Truffer, M. Fahenstock, and H. A. Fricker (2012), Analysis of low-frequency seismic signals generated during a multiple-iceberg calving event at Jakobshavn Isbrae, Greenland, *J. Geophys. Res.*, *117*, F01036, doi:10.1029/2011JF002132.
Walter, J. I., E. E. Brodsky, S. Tulaczyk, S. Y. Schwartz, and R. Pettersson (2011), Transient slip events from near-field seismic and geodetic data on a glacier fault, Whillans Ice Plain, West Antarctica, *J. Geophys. Res.*, *116*, doi:10.1029/2010JF001754.
West, M. E., C. F. Larsen, M. Truffer, S. O'Neel, and L. LeBlanc (2010), Glacier microseismicity, *Geology*, *38*(4), 319–322, doi:10.1130/G30606.1.
Wiens, D. A., S. Anandakrishnan, J. P. Winberry, and M. A. King (2008), Simultaneous teleseismic and geodetic observations of the stick–slip motion of an Antarctic ice stream, *Nature*, *453*(7196), 770–774, doi:10.1038/nature06990.
Winberry, J. P., S. Anandakrishnan, D. A. Wiens, R. B. Alley, and K. Christianson (2011), Dynamics of stick–slip motion, Whillans Ice Stream, Antarctica, *Earth Planet. Sci. Lett.*, *305*(3–4), 283–289, doi:10.1016/j.epsl.2011.02.052.
Winberry, J. P., S. Anandakrishnan, D. A. Wiens, and R. B. Alley (2013), Nucleation and seismic tremor associated with the glacial earthquakes of Whillans Ice Stream, Antarctica, *Geophys. Res. Lett.*, *40*, 312–315, doi:10.1002/grl.50130.
Zoet, L. K., S. Anandakrishnan, R. B. Alley, A. A. Nyblade, and D. A. Wiens (2012), Motion of an Antarctic glacier by repeated tidally modulated earthquakes, *Nat. Geosci.*, *5*(9), 623–626, doi:10.1038/ngeo1555.